A Hippocampus-Inspired Associative Memory Model Based on Spiking Neural Networks

Xinhua Bao[1], Jiaqiang Jiang[1], Junwei Cheng[1], Rui Yan[1*]
[1] College of Computer Science and Technology, Zhejiang University of Technology, Hangzhou, China
221124120134@zjut.edu.cn, jqjiang@zjut.edu.cn, 221124120123@zjut.edu.cn, ryan@zjut.edu.cn

***Abstract*—Associative memory is a fundamental cognitive function of the hippocampus and has been widely modeled using spiking neural networks (SNNs) combined with spike-timing-dependent plasticity (STDP). Existing memory models achieve effective associative recall through recurrent connectivity and synaptic plasticity. In this work, we propose a hippocampus-inspired associative memory model based on SNNs, incorporating three complementary mechanisms to regulate neuronal interaction and competition. We introduce a Top-K excitation circuit to selectively enhance excitatory coupling among recently active neurons. Second, the variable threshold mechanism dynamically adjusts neuronal excitability during learning. Third, an adaptive lateral inhibition mechanism is introduced, where neurons with higher accumulated activity receive stronger inhibition, while less active neurons are suppressed more weakly. Collectively, these mechanisms regulate neuronal interaction and competition within the memory module while remaining compatible with STDP. Experimental results demonstrate that the proposed model achieves robust associative memory retrieval under noisy and incomplete cues. Further analysis indicates that the introduced mechanisms promote more balanced neuronal activity and sparser synaptic utilization. Ablation studies demonstrate that the Top-K excitation circuit, the variable threshold mechanism, and the adaptive inhibition mechanism are complementary.**

***Index Terms*—Spiking Neural Networks, Associative Memory, Hippocampus-Inspired Model**

I. Introduction

Spiking Neural Networks (SNNs) [1] have emerged as a biologically inspired computational paradigm that processes information through discrete spike events and temporal dynamics. Among various learning rules, spike-timing-dependent plasticity (STDP) [2] has attracted significant attention due to its locality, temporal sensitivity, and biological plausibility. These properties make STDP a natural candidate for implementing associative memory [3], which aims to retrieve stored patterns from partial or noisy inputs.

Associative memory is closely related to hippocampal function in biological neural systems. Extensive studies have shown that the hippocampus plays a central role in memory formation and retrieval, supported by its characteristic trisynaptic circuit involving the dentate gyrus (DG), the cornu ammonis area 3 (CA3), and the cornu ammonis area 1 (CA1) [4]–[9]. This structure has inspired a variety of computational models that seek to capture key principles of hippocampal memory processing at different levels of abstraction, as demonstrated in [10]–[13]. In particular, the recurrent connectivity in CA3 is widely believed to support auto-associative memory, while DG contributes to pattern separation and CA1 facilitates pattern completion and readout. In these memory models, fixed firing thresholds are commonly used to control neuronal excitability, and lateral inhibition is typically implemented with static strength or uniform structure. Such design choices facilitate stable learning and efficient implementation, and these models can perform associative recall tasks in different settings. Depending on modeling objectives, existing approaches adopt different simplifications of hippocampal circuitry.

However, from a biological perspective, neuronal excitability and inhibitory effects in hippocampal circuits are inherently dynamic rather than static. Experimental studies indicate that neuronal firing thresholds can vary depending on recent membrane potential dynamics and spiking history [14], [15]. In addition, inhibitory interneurons in hippocampal regions such as CA1 exert heterogeneous influences on excitatory neurons, contributing to dynamic regulation of network activity [9]. These observations suggest that static designs in existing models may limit their ability to flexibly regulate neuronal participation during memory formation and recall.

Inspired by the hippocampus and the key-value architecture proposed in [16], we propose a hippocampus-inspired spiking associative memory model, consisting of a feature extraction module, a decoding module, and a memory module with three complementary mechanisms. First, an additional excitatory interaction pathway is introduced along the cognitive layer, and a Top-K excitation circuit is applied to selectively enhance excitatory coupling among a subset of active neurons based on recent activity. Second, the variable threshold mechanism is employed to dynamically adjust neuronal excitability during learning. Third, an adaptive lateral inhibition mechanism is incorporated to modulate inhibitory strength according to neuronal activity levels. Collectively, these mechanisms aim to regulate neuronal interaction and competition while remaining compatible with STDP-based learning.

The proposed model is evaluated on auto-associative and hetero-associative memory tasks using MNIST, EMNIST, and Fashion-MNIST datasets. Experimental results demonstrate robust memory retrieval under noisy and incomplete cues. Further analysis shows that the proposed mechanisms promote more balanced neuronal participation and sparser synaptic utilization. Ablation studies further verify the individual and complementary contributions of the proposed mechanisms.

This work was supported by the National Natural Science Foundation of China under Grant No. 62276235. *Corresponding Author

II. METHODS

A. Leaky Integrate-and-Fire Neuron and Gradient Update

We adopt the leaky integrate-and-fire (LIF) neuron model. The model was simulated with a time step Δt of 1 ms. The total synaptic input current is $I(t) = \sum_j w_j g_j(t)$, where w_j are the synaptic weights and $g_j(t)$ indicates the spike input from the other pre-synaptic neurons at time step t. In discrete time, the membrane potential update and spike generation can be written as:

$$v_j(t) = \alpha v_j(t-1) + (1-\alpha) I_j(t-1) - V_{th} g_j(t-1) \quad (1)$$

$$g_j(t) = \begin{cases} 1, & v_j(t) \geq V_{th} \\ 0, & \text{otherwise} \end{cases} \quad (2)$$

where $\alpha = \exp\left(-\frac{\Delta t}{\tau_m}\right)$. Here, $\tau_m = 20$ denotes the membrane time constant. A spike is generated when the membrane potential $v_j(t)$ crosses the threshold V_{th}, resulting in $g_j(t) = 1$. The gradient is computed via spatio-temporal backpropagation (STBP) [17] using the chain rule. However, the term $\frac{\partial g(t)}{\partial v(t)}$ is non-differentiable, so we adopt the surrogate gradient method, where $\theta = 1$, which is given by

$$\frac{\partial g(t)}{\partial v(t)} = \frac{1}{\theta} \text{sign}\left(|v(t) - V_{th}| < \frac{\theta}{2}\right) \quad (3)$$

Each spike leaves a trace $x_j(t)$ [18], which increases upon arrival of the spike $g_j(t)$ and decreases exponentially with time constant τ_s afterwards, which can be described as:

$$x_j(t) = (1 - e^{-\frac{1}{\tau_s}}) g_j(t) + e^{-\frac{1}{\tau_s}} x_j(t-1) \quad (4)$$

$$\Delta w_{ji}(t) = \beta_+ (w_{\max} - w_{ji}) x_j(t) x_i(t) - \beta_- w_{ji} x_j(t)^2 \quad (5)$$

This rule strengthens synapses for correlated spiking activity and weakens them otherwise.

B. Hippocampus-Inspired Memory Model

Our associative memory framework consists of three primary modules: a feature extraction module, a memory module, and a decoding module, as illustrated in Fig. 2.

The memory module contains four layers of LIF neurons: three excitatory layers and one inhibitory layer. Synaptic connections within this module are trained using the STDP learning rule. The first excitatory layer, referred to as the cognitive layer, continuously receives input from the feature extraction module and is connected to another excitatory layer. The second excitatory layer, termed the reactive layer, connects to the inhibitory layer. Importantly, the cognitive and reactive layers simultaneously receive feedforward input from the feature extractor, mimicking the pathway from Entorhinal Cortex (EC) to CA3 and CA1 during the memory phase. Finally, the output of the memory module is passed to the decoding module, which consists of three fully connected LIF layers, to decode and is reshaped to the final output.

In the memory phase, the memorized content, encoded and feature-extracted, is forwarded to the memory module, where synaptic weights are updated via STDP. Meanwhile, the remaining network components are trained via STBP. In the recall phase, when a cue is input into the memory model, the previously established synaptic weights enable activation of cognitive neurons in the memory layer. This activation, in turn, triggers the response of reactive neurons through the weight matrix w^m in the memory module, thus achieving memory recall. For clarity, we next introduce the three key mechanisms of the proposed hippocampus-inspired memory model.

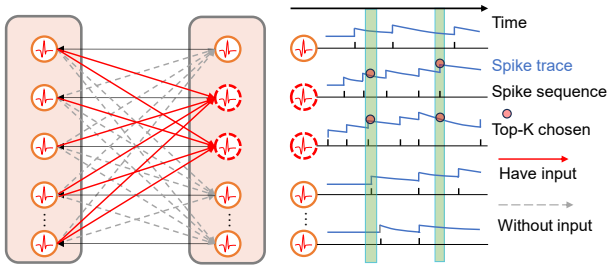

Fig. 1. The Top-K excitation circuit selects the Top-K neurons exhibiting the highest trace values and supplies them with additional excitatory input.

a) Top-K Excitation Circuit: Biologically, CA3 pyramidal neurons receive three major inputs: feedforward excitatory input from sensory pathways, recurrent excitatory input from other CA3 neurons, and inhibitory input from interneurons.

Inspired by this structure, we set the cognitive layer to receive data from the feature extraction module, and then establish a one-to-one pathway from cognitive neurons to excitatory neurons. Specifically, each excitatory neuron is connected to all cognitive neurons except the one that provides its input. Considering the critical regulatory role of inhibitory neurons in CA3, we further introduce a Top-K excitation circuit that acts on the cognitive layer. As illustrated in Fig. 1, at each time step, the traces of cognitive neurons are used to identify the Top-K most active neurons, which receive additional excitatory synaptic inputs, while the others do not receive extra excitation input. The input current received by cognitive neurons can be formulated as follows:

$$Mask_i(t) = TopK(x_i(t)) \quad (6)$$

The selected Top-K neurons are assigned a value of 1 in $Mask_i(t)$, while the others are set to 0 and K is set to 90.

$$I_i^c(t) = \sum_h w_{i,h} g_h(t) + Mask_i(t) \odot \sum_k w_{i,k} g_k(t) \quad (7)$$

Here, $I_i^c(t)$ denotes the input current to cognitive neuron i at time step t. The $g_h(t)$ represents the spike output of neuron h in the final layer of the feature extraction module, and $w_{i,h}$ denotes the synaptic weight from pre-synaptic neuron h to post-synaptic neuron i. Likewise, $g_k(t)$ is the spike activity of neuron k in the excitatory layer, and $w_{i,k}$ represents the synaptic weight from neuron k to neuron i. Through this mechanism, the Top-K excitation circuit enhances transient competition and cooperation among cognitive neurons, promoting representational separability during memory encoding. Here, $\odot$ denotes the Hadamard product.

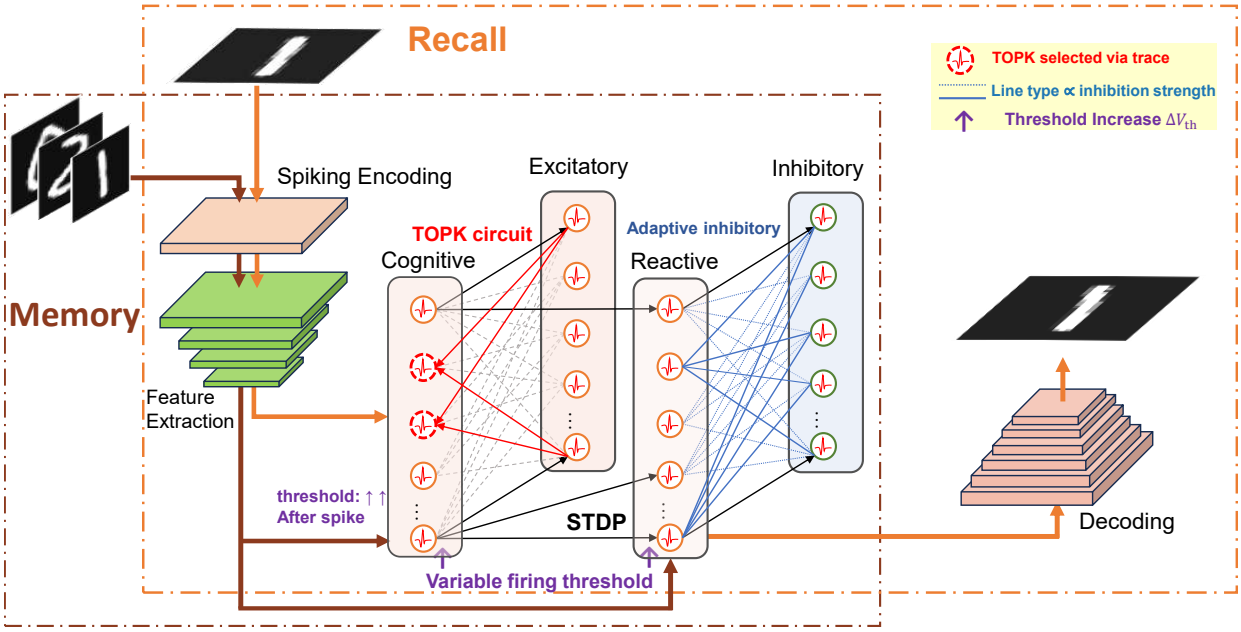

Fig. 2. The model consists of three components: a feature extraction module (left, green), a memory module (middle) comprising cognitive, reactive, excitatory, and inhibitory neurons, and a decoding module (right, pink). During the memory phase (brown border), the encoded and feature-extracted sequential data are subsequently sent to the cognitive and reactive neurons. We then establish a one-to-one pathway from cognitive neurons to excitatory neurons. Each excitatory neuron is connected to all cognitive neurons except the one that provides its input, while only Top-K selected neurons get additional input, which is computed by $x_i(t)$ in a single time step (red lines). Similarly, connections in reactive neurons and inhibitory neurons, where the inhibition strength is determined by the $SpikeCount$ (blue lines; line type indicates the strength of inhibition). The variable threshold mechanism is employed in both cognitive and reactive neurons. After each spike, the neuron's threshold will increase. With these mechanisms and the STDP learning rule, the synaptic weight matrix w^m is established between the cognitive and reactive neurons. During the recall phase (orange border), randomly selected samples from previous inputs are processed and sent to the cognitive neurons. The cognitive neurons activate the reactive neurons through w^m, and finally, the decoding module reconstructs the retrieved content. Threshold is reset at the beginning of the next memory phase in the next epoch.

b) Variable Threshold Mechanism: From a biological perspective, neuronal firing thresholds in the brain are not fixed; instead, they vary dynamically according to neurons' recent activity history. We observe that certain neurons in the cognitive layer develop stronger synaptic weights than others, enabling them to dominate network dynamics under STDP rule. This imbalance can interfere with accurate memory retrieval by biasing the network toward a subset of highly active neurons. Therefore, we apply a simple but effective variable threshold mechanism for spiking neurons, as illustrated in Fig. 3. For simplicity, we also employ an irreversible linear adaptation method, in which the firing threshold of a neuron progressively increases with its activity and does not decay

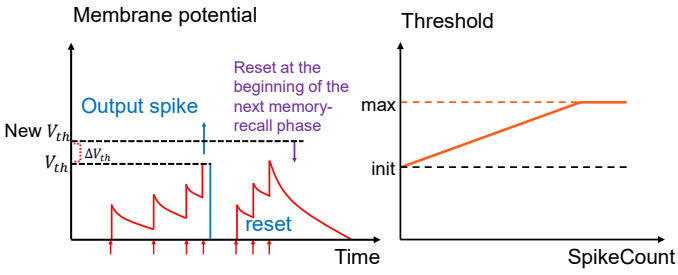

Fig. 3. The left panel shows the membrane potential dynamics over time. After a spike occurs, the firing threshold increases by ΔV_{th} until it reaches a maximum value, and V_{th} is reset at the beginning of the next memory phase.

over time. Importantly, the variable threshold mechanism is reset to its initial value at the onset of each subsequent memory-recall phase and is exclusively applied within the memory module. By contrast, neurons in the encoder, feature extraction module, and decoder retain fixed firing thresholds. The variable threshold can be calculated as follows:

$$V_{th} = min(V_{init} + \lambda(V_{max} - V_{init})SpikeCount_j(t), V_{max}) \tag{8}$$

As illustrated in Fig. 3 and Equation 8, the firing threshold is initially set to $V_{init} = 0.05$, where $SpikeCount_j(t)$ denotes the cumulative number of spikes generated by neuron j up to time t. Each time a neuron emits a spike, its threshold increases proportionally by a factor of $\lambda(V_{max} - V_{init})$, where $\lambda = 0.01$ controls the adaptation rate, and $V_{max} = 0.075$ is an upper bound on the firing threshold. If λ is too large, the threshold rises too quickly, excessively suppressing highly active neurons and consequently degrading network performance. Conversely, if λ is too small, the adaptive mechanism becomes ineffective at mitigating activity imbalance.

As a result, persistently active neurons become increasingly difficult to fire, which suppresses their dominance and encourages less active neurons to participate in memory encoding.

c) Adaptive Lateral Inhibition Mechanism: In memory models, lateral inhibition plays a critical role in regulating competition among excitatory neurons. Similarly to the cognitive layer, the reactive layer also has one-to-one connec-

tions from reactive neurons to inhibitory neurons, and each inhibitory neuron inhibits other reactive neurons excluding the one that activated itself. Conventional lateral inhibition, which is analogous to the soft winner-take-all (soft-WTA) mechanism, provides approximately uniform inhibition and may fail to prevent highly active neurons from repeatedly dominating memory retrieval. Thus, we introduce the adaptive lateral inhibitory mechanism, which applies different degrees of inhibition to different reactive neurons each time, and this effect varies dynamically according to each neuron's firing history, which can be described as:

$$Mask_j(t) = \frac{SpikeCount_j(t)}{max(SpikeCount_j(t)) + \epsilon} \tag{9}$$

$$I_j^r(t) = \sum_h w_{j,h} g_h(t) + \sum_i w_{j,i} g_i(t) - Mask_j(t) \sum_p w_{j,p} g_p(t) \tag{10}$$

Formally, $I_j^r(t)$ denotes the input current to reactive neuron j at time t. The terms $g_h(t)$ and $g_i(t)$ represent spikes from neuron h in the final layer of the feature extraction module and cognitive neuron i, respectively, while $g_p(t)$ denotes the spike output of inhibitory neuron p. The associated synaptic weights are $w_{j,h}$, $w_{j,i}$, and $w_{j,p}$. $SpikeCount_j(t)$ denotes the total number of spikes emitted by reactive neuron j up to time t. We first compute the maximum spike number among all reactive neurons. An adaptive inhibition coefficient is then obtained by normalizing each neuron's spike number by this maximum value. A small constant $\epsilon = 1 \times 10^{-8}$ is added to avoid division by zero. This coefficient is applied through a Hadamard product to scale the inhibitory input received by each reactive neuron, thereby achieving adaptive lateral inhibition that neurons with higher accumulated activity receive proportionally stronger inhibition, while less active neurons are suppressed more weakly as illustrated in Fig. 4.

III. Experimental Results

In an auto-associative memory task, a sequence of images is continuously presented to the model, and the stored patterns can be successfully retrieved when an appropriate cue is provided [19]. The hetero-associative memory task takes different types of input, such as text, as input to the memory model, and then it can retrieve the corresponding picture. In the experimental section, we evaluate the proposed memory model on these tasks to demonstrate its ability to store and retrieve information. We further assess the robustness of the model under noisy inputs, as well as its pattern separation and completion capabilities. Finally, ablation studies are conducted to verify the effectiveness of the proposed mechanisms. To assess the effectiveness of each proposed mechanism, a vanilla model with identical architecture and training settings, but without the proposed mechanisms, is used as a baseline for comparison.

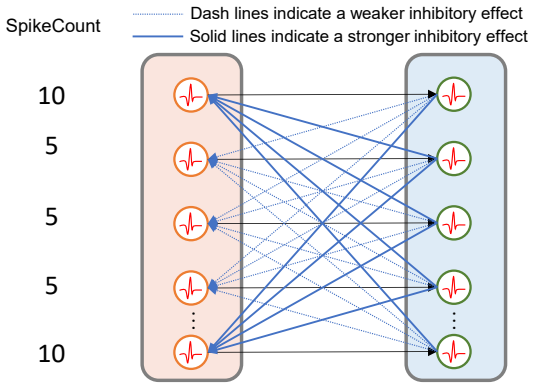

Fig. 4. The figure shows that the inhibition strength depends on the $SpikeCount$. Dash lines corresponding to lower $SpikeCount$ indicate a weaker inhibitory effect, while solid lines indicate the opposite.

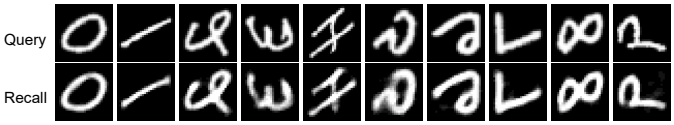

Fig. 5. The recalled image (Recall) is the memorized image corresponding to the query image on the EMNIST dataset.

A. Auto-associative and Hetero-associative Memory

For the auto-associative memory task, we select images from 10 different classes in the MNIST and EMNIST datasets [20], [21]. For the hetero-associative memory task, we construct text-image pairs using 5 different classes from the Fashion-MNIST dataset [22], where class labels are converted into textual representations paired with their corresponding images. The cognitive and reactive layers consist of 100 neurons in two tasks. The sequential memory stream contains 3000 training samples and 1000 test samples, randomly drawn from the selected categories. After 150 training epochs, we present the final recall results along with the corresponding original memorized content for comparison. In addition, a Spiking TextCNN [11] is used to establish the hetero-associative mapping between textual inputs and images.

In both associative memory tasks, the memorized content is first encoded into spikes and sent to the corresponding feature extractor, then the memory module receives the data, and STDP rule is employed to dynamically establish synapses between the neurons. After the network finishes training, we send a query image, randomly chosen from memory images, to the memory model and the model recalls the image corresponding

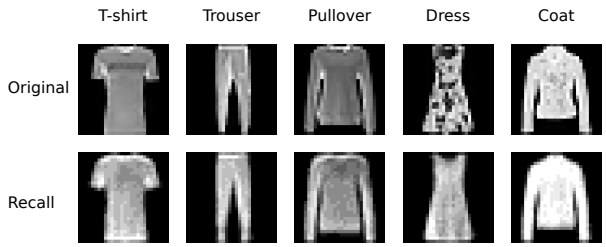

Fig. 6. The reconstruction results of each image recalled by the model after inputting different text during the query process.

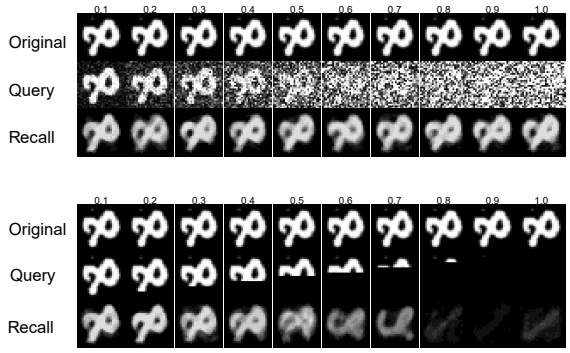

Fig. 7. The examples of model reconstruction under different levels of Gaussian noise (top) and occlusion (bottom), demonstrating the model's pattern completion capability.

to the query in the auto-associative memory task. Similarly, we send the text as a cue and the model reconstructs the corresponding image in the hetero-associative memory task. The results are shown in Fig. 5 and Fig. 6, which demonstrate that the model can successfully retrieve stored patterns.

B. Results under Different Image Perturbations

To evaluate the robustness of the proposed model, we conducted two groups of experiments. In the first experiment, the memory model was trained using clean data. After inputting the memory images into the network, the query images are corrupted using additive Gaussian noise or random masking at 10 different intensity levels to assess the model's pattern completion capability, as presented in Fig. 7, which suggests that the memory module can effectively retrieve complete patterns from incomplete or degraded inputs.

In the second experiment, Gaussian noise with a standard deviation of 0.01 was added to both the training and the test datasets. The SSIM of vanilla and ours are 0.70 and 0.82, respectively. Furthermore, t-distributed Stochastic Neighbor Embedding (t-SNE) was used to analyze the learned representations and evaluate pattern separation. As illustrated in Fig. 8, the proposed model produces well-separated clusters.

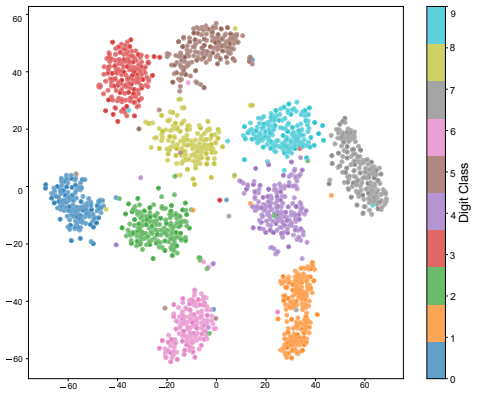

Fig. 8. The t-SNE visualization demonstrates that the memory model exhibits strong pattern separation capability.

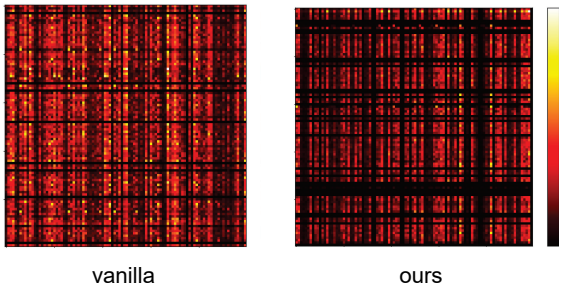

Fig. 9. The figure shows that, with the proposed mechanisms, the weight matrix w^m becomes sparser and no longer contains excessively large synaptic values; the number of small yellow dots in the graph is significantly reduced.

C. Analysis of the Hippocampus-Inspired Memory Model

To further analyze the internal behavior of the proposed model, we examined synaptic utilization and neural activity statistics in the associative memory task. We define synaptic utilization as the fraction of established synapses between the two layers of all possible synaptic connections in w^m. As cognitive neurons establish unidirectional synaptic connections to reactive neurons, we calculate the maximum values of these synaptic strengths for cognitive neurons and reactive neurons in the memory phase, and the average firing rates of them in the recall phase. Two heatmaps of the memory weight matrices w^m for the proposed model and the vanilla model are shown in Fig. 9. The proposed model exhibits noticeably sparser synaptic connectivity under the same task conditions compared to the vanilla model. Specifically, the maximum cognitive synaptic strength decreases from 18.26 to 8.59, and the average cognitive firing rate decreases from 0.0165 to 0.0146. In contrast, the maximum reactive synaptic strength increases from 9.18 to 10.93. Moreover, synaptic utilization is reduced from 67% to 46%, while the average SSIM improves from 0.82 to 0.85. These results indicate that the proposed mechanisms promote sparser yet more effective synaptic representations, leading to improved memory quality.

D. Ablation Study

We conduct ablation studies based on auto-associative memory tasks, in which each model needed to memorize images from 10 categories. As our framework introduces three mechanisms, we evaluate their contributions individually.

As shown in Table I, the maximum cognitive synaptic strength reaches 18.26. These highly active neurons repeatedly dominate the competition, and under the STDP learning rule their synaptic weight strengths continue to increase, leading to activity imbalance. After introducing the variable threshold mechanism, these neurons become progressively harder to activate, resulting in a reduced firing rate and a more balanced participation between neurons. This result indicates that the Top-K mechanism does not simply increase overall excitation; rather, it sharpens instantaneous competition, enhances representational separability, as shown in Fig. 8 and Fig. 9. Next,

TABLE I
ABLATION STUDY ON TOP-K EXCITATION CIRCUIT

Method	Max cognitive strength	Average cognitive firing rate	Synaptic utilization(%)
Fix+Inh (vanilla)	18.26	0.0165	67
VariThr+AdptInh+w/o TK	10.39	0.0156	54
VariThr+AdptInh+w/ TK=90	8.59	0.0146	46

TABLE II
ABLATION STUDY ON ADAPTIVE LATERAL INHIBITION

Method	Max reactive strength	Average reactive firing rate	Synaptic utilization(%)
Fix+Inh (vanilla)	9.18	0.0532	67
VariThr+Inh	11.47	0.0512	57
VariThr+AdptInh	10.90	0.0601	54

we evaluate the variable threshold mechanism by comparing two models trained on MNIST: one with the variable threshold and one with a fixed threshold. And the model with variable threshold consistently achieves higher SSIM values, improving from 0.81 to 0.85. This demonstrates that variable thresholding improves memory recall quality. Finally, we examine the adaptive lateral inhibition mechanism. Since the inhibition coefficient is computed from $SpikeCount$, which is influenced by $MaxSpikes$. Therefore, these two mechanisms are evaluated jointly in this ablation setting, as shown in Table II. When only the variable threshold mechanism is applied, highly active neurons gradually increase their firing thresholds until V_{max}. However, reactive neurons are still subjected to approximately uniform lateral inhibition. In contrast, when inhibition strength is dynamically modulated according to relative spike activity, highly active neurons receive stronger inhibition while less active neurons receive weaker inhibition. This enables more reactive neurons to participate in memory encoding, leading to sparser synaptic connectivity and a reduction in the average reactive synaptic strength.

Overall, the ablation results demonstrate that the variable threshold mechanism plays a dominant role in stabilizing neural activity and improving reconstruction quality, while the Top-K excitation and adaptive lateral inhibition mechanism provide complementary benefits.

IV. CONCLUSION

In this work, we propose a hippocampus-inspired associative memory model based on SNNs. The core objective of the proposed approach is to dynamically regulate neuronal activity and competition during memory encoding and recall. The model incorporates several biologically inspired mechanisms, including a Top-K excitation circuit, the variable threshold mechanism, and an adaptive lateral inhibition mechanism. Collectively, these components promote more balanced neuronal participation and sparser synaptic utilization. We evaluate the model on auto- and hetero-associative memory tasks using EMNIST, Fashion-MNIST and MNIST datasets, and results demonstrate the effectiveness of the proposed mechanisms, and ablation studies further verify the contributions of them.

REFERENCES

[1] W. Maass, "Networks of spiking neurons: the third generation of neural network models," *Neural networks*, vol. 10, no. 9, pp. 1659–1671, 1997.

[2] G.-q. Bi and M.-m. Poo, "Synaptic modifications in cultured hippocampal neurons: dependence on spike timing, synaptic strength, and postsynaptic cell type," *Journal of neuroscience*, vol. 18, no. 24, pp. 10 464–10 472, 1998.

[3] J. J. Hopfield, "Neural networks and physical systems with emergent collective computational abilities." *Proceedings of the national academy of sciences*, vol. 79, no. 8, pp. 2554–2558, 1982.

[4] R. P. Kesner, I. Lee, and P. Gilbert, "A behavioral assessment of hippocampal function based on a subregional analysis," *Reviews in the Neurosciences*, vol. 15, no. 5, pp. 333–352, 2004.

[5] A. Treves and E. T. Rolls, "Computational analysis of the role of the hippocampus in memory," *Hippocampus*, vol. 4, no. 3, pp. 374–391, 1994.

[6] V. Cutsuridis, S. Cobb, and B. P. Graham, "Encoding and retrieval in a model of the hippocampal ca1 microcircuit," *Hippocampus*, vol. 20, no. 3, pp. 0–0, 2010.

[7] D. Marr, "Simple memory: a theory for archicortex," *Philosophical Transactions of the Royal Society of London. B, Biological Sciences*, vol. 262, no. 841, pp. 23–81, 1971.

[8] T. F. Freund and G. Buzsáki, "Interneurons of the hippocampus," *hippocampus*, vol. 6, no. 4, pp. 347–470, 1996.

[9] K. A. Pelkey, R. Chittajallu, M. T. Craig, L. Tricoire, J. C. Wester, and C. J. McBain, "Hippocampal gabaergic inhibitory interneurons," *Physiological reviews*, vol. 97, no. 4, pp. 1619–1747, 2017.

[10] D. Casanueva-Morato, A. Ayuso-Martinez, J. P. Dominguez-Morales, A. Jimenez-Fernandez, and G. Jimenez-Moreno, "A bio-inspired implementation of a sparse-learning spike-based hippocampus memory model," *IEEE Transactions on Emerging Topics in Computing*, vol. 13, no. 1, pp. 119–133, 2024.

[11] W. Jiang, L. Wang, L. Qin, and R. Yan, "Stdp-based associative memory model on spiking neural networks," in *2024 International Joint Conference on Neural Networks (IJCNN)*. IEEE, 2024, pp. 1–8.

[12] C. H. Tan, H. Tang, K. C. Tan, and M. Yuan, "A hippocampus ca3 spiking neural network model for storage and retrieval of sequential memory," in *2013 IEEE Conference on Cybernetics and Intelligent Systems (CIS)*. IEEE, 2013, pp. 134–139.

[13] C. H. Tan, H. Tang, E. Y. Cheu, and J. Hu, "A computationally efficient associative memory model of hippocampus ca3 by spiking neurons," in *The 2013 International Joint Conference on Neural Networks (IJCNN)*, 2013, pp. 1–8.

[14] D. A. Henze and G. Buzsáki, "Action potential threshold of hippocampal pyramidal cells in vivo is increased by recent spiking activity," *Neuroscience*, vol. 105, no. 1, pp. 121–130, 2001.

[15] W. B. Wilent and D. Contreras, "Stimulus-dependent changes in spike threshold enhance feature selectivity in rat barrel cortex neurons," *The Journal of Neuroscience*, vol. 25, no. 11, pp. 2983–2991, 2005. [Online]. Available: https://www.jneurosci.org/content/25/11/2983

[16] T. Limbacher, O. Özdenizci, and R. Legenstein, "Memory-dependent computation and learning in spiking neural networks through hebbian plasticity," *IEEE Transactions on Neural Networks and Learning Systems*, 2023.

[17] Y. Wu, L. Deng, G. Li, J. Zhu, and L. Shi, "Spatio-temporal backpropagation for training high-performance spiking neural networks," *Frontiers in neuroscience*, vol. 12, p. 331, 2018.

[18] A. Morrison, M. Diesmann, and W. Gerstner, "Phenomenological models of synaptic plasticity based on spike timing," *Biological cybernetics*, vol. 98, no. 6, pp. 459–478, 2008.

[19] H.-G. Yoon and P. Kim, "An stdp-based encoding method for associative and composite data," *Scientific Reports*, vol. 12, no. 1, p. 4666, 2022.

[20] Y. LeCun, L. Bottou, Y. Bengio, and P. Haffner, "Gradient-based learning applied to document recognition," *Proceedings of the IEEE*, vol. 86, no. 11, pp. 2278–2324, 2002.

[21] G. Cohen, S. Afshar, J. Tapson, and A. Van Schaik, "Emnist: Extending mnist to handwritten letters," in *2017 international joint conference on neural networks (IJCNN)*. IEEE, 2017, pp. 2921–2926.

[22] H. Xiao, K. Rasul, and R. Vollgraf, "Fashion-mnist: a novel image dataset for benchmarking machine learning algorithms," *arXiv preprint arXiv:1708.07747*, 2017.